A Mixed-Integer Linear Programming Model for the Electric Vehicle Charging Coordination Problem in Unbalanced Electrical Distribution Systems

John F. Franco, *Member, IEEE,* Marcos J. Rider, *Member, IEEE,* and Ruben Romero, *Senior Member, IEEE.*

***Abstract*—This paper presents a novel mixed-integer linear programming (MILP) model for the electric vehicle charging coordination (EVCC) problem in unbalanced electrical distribution systems (EDSs). Linearization techniques are applied over a mixed-integer nonlinear programming model to obtain the proposed MILP formulation based on current injections. The expressions used to represent the steady-state operation of the EDS take into account a three-phase representation of the circuits, as well as the imbalance of the loads, leading to a more realistic model. Additionally, the proposed formulation considers the presence of distributed generators and operational constraints such as voltage and current magnitude limits. The optimal solution for the mathematical model was found using commercial MILP solvers. The proposed formulation was tested in a distribution system used in the specialized literature. The results show the efficiency and the robustness of the methodology, and also demonstrate that the model can be used in the solution of the EVCC problem in EDSs.**

***Index Terms*—Electric vehicles charging coordination (EVCC), mixed integer linear programming (MILP), unbalanced electrical distribution systems (EDSs).**

NOMENCLATURE

Sets

F	Sets of phases {A,B,C}.
L	Sets of circuits.
N	Sets of nodes.
T	Sets of time intervals.

Constants

$\alpha^{G}_{n,t}$	Energy cost at node n in time period t.
β	Electric vehicle (EV) energy curtailment cost.
Δ_t	Duration of the time interval t.
$\overline{\delta}_{mn}$	Discretization step for the current of circuit mn.
κ_n	Parameter that indicates if there is a priority EV at node n.
$\overline{\lambda}$	Number of blocks of the square current piecewise linearization.
θ	Vector of reference phase angles.
θ_1	Maximum negative deviation of the phase angle around the reference angle for each phase.
θ_2	Maximum positive deviation of the phase angle around the reference angle for each phase.
ρ_t	Parameter used to encourage the charging of a priority EV as soon as possible.
$\sigma_{mn,\lambda}$	Slope of the λth block of the piecewise linearization for the current of circuit mn.
$B_{mn,f}$	Shunt susceptance of circuit mn for phase f.
$\overline{E}^{\mathrm{EV}}_{n}$	Energy capacity of EV at node n.
E^{SoC}_{n}	Initial charge state of EV at node n.
$\overline{I}_{mn}$	Maximum current flow magnitude of circuit mn.
$P^{D}_{n,f,t}$	Active power demand at node n for phase f in time interval t.
$\overline{P}^{\mathrm{EV}}_{n}$	Maximum power consumption of EV at node n.
pf_n	Minimum power factor for the operation of distributed generator (DG) at node n.
$\overline{P}^{G}_{n}$	Maximum active power of DG at node n.
$Q^{D}_{n,f,t}$	Reactive power demand at node n for phase f in time interval t.
$\overline{Q}^{G}_{n}$	Maximum reactive power of DG at node n.
$\underline{Q}^{G}_{n}$	Minimum reactive power of DG at node n.
$R_{mn,f,h}$	Resistance of circuit mn between phases f and h.
S	Substation node.
t^{arr}_{n}	Estimated arrival time for EV at node n.
t^{dep}_{n}	Estimated departure time for EV at node n.
$\overline{V}$	Maximum voltage magnitude limit.
$\underline{V}$	Minimum voltage magnitude limit.
$V^{\mathrm{re}^*}_{n,f,t}$	Real part of the estimated voltage at node n for phase f in time interval t.
$V^{\mathrm{im}^*}_{n,f,t}$	Imaginary part of the estimated voltage at node n for phase f in time interval t.
$X_{mn,f,h}$	Reactance of circuit mn between phases f and h.

Variables

$\delta_{mn,f,t,\lambda}$	Value of the λth block of the piecewise linearization for the current of circuit mn for phase f in time interval t.
E^{EV}_{n}	Energy of EV at node n at the end of the time period.
E^{SH}_{n}	Energy curtailment of EV at node n at the end of the time period.

Manuscript received May 19, 2014; revised September 30 2014 and November 27, 2014; accepted January 15, 2015. Date of publication February 4, 2015; date of current version August 19, 2015. This work was supported by the Brazilian Institutions Conselho Nacional de Desenvolvimento Científico e Tecnológico and Fundação de Amparo á Pesquisa do Estado de São Paulo (FAPESP) under Grant 2012/01100-6. Paper no. TSG-00477-2014.

The authors are with the Department of Electrical Engineering, São Paulo State University (FEIS-UNESP), Ilha Solteira 15385-000, Brazil (e-mail: jffranco@gmail.com).

Color versions of one or more of the figures in this paper are available online at http://ieeexplore.ieee.org.

Digital Object Identifier 10.1109/TSG.2015.2394489

$I^{\mathrm{Dim}}_{n,f,t}$ Imaginary part of the current demanded by a conventional load at node n for phase f in time interval t.
$I^{\mathrm{Dre}}_{n,f,t}$ Real part of the current demanded by a conventional load at node n for phase f in time interval t.
$I^{\mathrm{EVim}}_{n,f,t}$ Imaginary part of the current demanded by the EV at node n for phase f in time interval t.
$I^{\mathrm{EVre}}_{n,f,t}$ Real part of the current demanded by the EV at node n for phase f in time interval t.
$I^{\mathrm{Gim}}_{n,f,t}$ Imaginary part of the current generated at node n for phase f in time interval t.
$I^{\mathrm{Gre}}_{n,f,t}$ Real part of the current generated at node n for phase f in time interval t.
$I^{\mathrm{im}}_{mn,f,t}$ Imaginary part of the current in circuit mn for phase f in time interval t.
$I^{\mathrm{im}+}_{mn,f,t}$ Positive component of the current's imaginary part in circuit mn for phase f in time interval t.
$I^{\mathrm{im}-}_{mn,f,t}$ Negative component of the current's imaginary part in circuit mn for phase f in time interval t.
$I^{\mathrm{re}}_{mn,f,t}$ Real part of the current in circuit mn for phase f in time interval t.
$I^{\mathrm{re}+}_{mn,f,t}$ Positive component of the current's real part in circuit mn for phase f in time interval t.
$I^{\mathrm{re}-}_{mn,f,t}$ Negative component of the current's real part in circuit mn for phase f in time interval t.
$I^{\mathrm{sqr}}_{mn,f,t}$ Square of the current in circuit mn for phase f in time interval t.
$P^{\mathrm{EV}}_{n,t}$ Active power consumption of EV at node n in time interval t.
$P^{G}_{n,t}$ Active power generated at node n in time interval t.
$Q^{G}_{n,t}$ Reactive power generated at node n in time interval t.
$V^{\mathrm{re}}_{n,f,t}$ Real part of the voltage at node n for phase f in time interval t.
$V^{\mathrm{im}}_{n,f,t}$ Imaginary part of the voltage at node n for phase f in time interval t.
$y_{n,t}$ Binary variable associated to the charging state of the EV at node n in time interval t.

I. Introduction

THE USE of EVs will increase over the coming years, with the aim of reducing the green-house gas emissions and taking advantage of renewable power sources [1], [2]. EVs have batteries that allow them to store the energy needed for transportation. Those batteries can be charged in the electrical distribution system (EDS). Uncoordinated charging can cause several problems in the EDS, such as overloads, voltage limits violations, and excessive increase in power losses [3], [4]. For this reason, coordination is necessary to adequately charge the EVs, while maintaining the quality operation of the EDS. By taking advantage of the communication infrastructure of forthcoming smart grids, the EDS operator can control the charging of each vehicle according to a set schedule coordination for all of the EVs in the system [5].

The EV charging coordination (EVCC) problem deals with finding an optimal charging schedule for the EVs' batteries, in order to achieve economical operation of the EDS, while satisfying operational constraints. Optimal charging scheduling must maximize the energy charged to the batteries and minimize power losses. Several works have addressed the charging coordination problem of EVs in EDSs [3]–[6]. A mixed-integer linear programming (MILP) formulation that used detailed information on battery charging profiles was proposed in [6]; the objective of that model was to optimize charging costs, but the impact of the EVs on the grid was not considered.

A real-time smart load management algorithm was applied to the optimal charging of EVs in [7]. This method aimed at improving the reliability and security of the EDS by minimizing voltage deviation, overload, and power losses compared to a noncoordinated recharging scheme for the EVs. It was assumed that there was a two-way communication infrastructure between the system operation center and the recharging points, which made it possible to control the EV recharging process. The algorithm divided the time period into intervals, allowing users to establish priorities in the selection of the charging intervals; in each step of the algorithm a sensitivity index was used to identify the more appropriate EV to be recharged with the objective of causing less of an increase in power losses.

In [8], a linear programming formulation for the optimal charging of EVs was proposed; the mathematical model was formulated considering network sensitivities, rather than including the network equations themselves. An agent-based transportation micro-simulation was used in [9] to provide detailed temporal and spatial information about the behavior EVs exhibit to guarantee secure system operation. An analysis of the EV integration with the power system was made in [10]. This paper demonstrated that EVs that are able to transfer power to the grid, known as vehicle-to-grid (V2G), can provide power regulation, allowing the system operator to use the energy stored in the EVs' batteries. In effect, it is possible to reduce the power reserve needed from conventional energy resources by using aggregated energy of the EVs.

If a communication infrastructure exists, the EV recharging rate can be controlled and the power regulation, as an ancillary service, can be accomplished by changing the recharging rate of each EV around an established operation point [11]. Using an aggregation scheme, it is possible to combine the capacities of multiple EVs, in order to participate in a power reserve market. In [12], a mathematical optimization model was developed with the aim of maximizing the revenue obtained by employing the contributions of power reserve for frequency control. An aggregator controlled the power direction (consumption or supplying) of V2G, in order to provide that regulation service. In that work, optimal charging algorithms were proposed to define the optimal operation point of the EVs, with the objective of maximizing the payments associated with the power regulation service.

A framework for optimizing both the charging and the power management of an EV based in dynamic programming was presented in [13]. Both issues were optimized

simultaneously, in order to avoid any loss of optimality that may have resulted from solving them separately. A decision model to implement direct load control over the battery charging process was developed in [14]. The energy supplied to the EVs was maximized, while global energy costs were minimized. That model was a MILP formulation that considered three types of energy management decisions: 1) grid-to-vehicle charges; 2) V2G discharges; and 3) vehicle-to-vehicle energy exchanges. However, the formulation does not take into account the network equations to evaluate the EDSs state of operation.

The flexible charging capability of EVs was considered in [15] in order to propose a novel pool market mechanism aimed at including demand side integration in electricity markets. A framework employing neural networks was used to predict the energy consumption of an EV over a route [16]. The findings confirmed that being able to estimate the EVs energy requirements for a given route is necessary for developing an efficient charge control strategy. The real-time energy management algorithm considering EVs and photovoltaic systems, proposed in [17], employed a fuzzy controller to manage the uncertain variables involved in the energy exchange process. A decentralized approach to EV charge management was proposed in [18]. In that work, EV charging was requested and approved for limited time periods.

A novel MILP model for the EVCC problem in unbalanced EDSs is proposed in this paper. Linearization techniques, such as the piecewise and linear approximations of nonlinear functions, are applied to a mixed-integer nonlinear programming (MINLP) model to obtain the proposed MILP formulation. Current injections, along with a three-phase representation of the circuits are used to represent the steady-state operation of an unbalanced EDS. In the proposed formulation, the power of DGs and operational constraints are also taken into account. The optimal solution of the model is found by using commercial MILP solvers that, can guarantee the optimal solution for MILP models. The proposed model was tested in a 394-node distribution system. The results show the efficiency and the robustness of the methodology.

The main contributions of this paper are as follows:

1) a new set of equations that represents the steady state operation of an unbalanced EDS considering the presence of DGs;
2) a MINLP model for the EVCC problem that takes into account the imbalance of the EDS;
3) a MILP formulation for the EVCC problem that can be solved using commercial solvers.

II. EVCC Problem

The EVCC problem is to determine an EV battery charging schedule so that the EDS operates with optimal cost and satisfies operational constraints. In this paper, the following are assumed.

1) The EV batteries must be charged in a given period of time, which is divided into several time intervals.
2) The energy required by each battery is known at the beginning of the time period.
3) The EVs have communication devices that allow the EDS operator to control the charging state of the batteries. That control can be carried out in each time interval of the time period.

Operational constraints, such as voltage magnitude limits, power generation limits, and maximum circuit currents must be satisfied. The optimal charging schedule defines the charging state of each EV battery in each time interval. The charging state of an EV battery can be represented by a binary variable $y_{n,t}$ that has a value of 1 if the battery is charging at its maximum power $\overline{P}_n^{\mathrm{EV}}$ and a value of 0 if the battery is not charging.

The estimated arrival and departure times for the EVs are considered using parameters t_n^{arr} and t_n^{dep}, respectively. These parameters, as well as the initial charge state of an EV (E_n^{SoC}), can be obtained using estimation techniques applied to EVs, such as those in [19]–[21]. The mathematical model considers these parameters, allowing the EV to be charged only during the time interval between arrival and departure.

The model proposed in this paper takes into account charging priorities selected by the users. These priority considerations allows the users to charge their EVs as quickly as possible, even if the energy cost is larger. This option offers the users flexibility, because it guarantees that the EV will be available as soon as possible.

III. MINLP Model for the EVCC Problem

The EVCC problem can be modeled as a MINLP problem using (1)–(21). The EDS is modeled as an unbalanced system, in which the conventional loads and the circuits are considered using a three-phase representation. Additionally, the active and reactive power injections of DGs are taken into account and the loads are modeled as a constant power type. It is assumed that the recharging period lasts from 18:00 to 08:00 h. This time period is divided into several time intervals (set T); the time interval that begins at time t is associated with the element t of the set T and has a time duration equal to Δ_t.

The proposed optimization model aims to minimize the energy cost of EV charging, which usually implies charging during the final hours of the time period (due to the lower cost of energy at that time). However, with the objective of adding flexibility to the EV charging process, the charging of some EVs can be prioritized if requested by their owners. Priority EVs will be charged as quickly as possible, despite the fact that the energy cost is usually higher in the first hours of the time period

$$\min \sum_{f\in F}\sum_{t\in T}\alpha_{S,t}^{G}\Delta_t\left(V_{S,f,t}^{\mathrm{re}}I_{S,f,t}^{\mathrm{Gre}}+V_{S,f,t}^{\mathrm{im}}I_{S,f,t}^{\mathrm{Gim}}\right)+\sum_{n\in N}\sum_{t\in T}\alpha_{n,t}^{G}\Delta_t P_{n,t}^{G}+\sum_{n\in N}\beta E_n^{SH}-\sum_{n\in N}\sum_{t\in T}\kappa_n\rho_t P_{n,t}^{\mathrm{EV}} \quad (1)$$

subject to

$$I^{\mathrm{Gre}}_{m,f,t} + \sum_{km\in L} I^{\mathrm{re}}_{km,f,t} - \sum_{mn\in L} I^{\mathrm{re}}_{mn,t} - \left(\sum_{km\in L} B_{km,f} + \sum_{mn\in L} B_{mn,f}\right)\frac{V^{\mathrm{im}}_{m,f,t}}{2} = I^{\mathrm{Dre}}_{m,f,t} + I^{\mathrm{EVre}}_{m,f,t} \quad \forall m \in N, f \in F, t \in T \quad (2)$$

$$I^{\mathrm{Gim}}_{m,f,t} + \sum_{km\in L} I^{\mathrm{im}}_{km,f,t} - \sum_{mn\in L} I^{\mathrm{im}}_{mn,t} - \left(\sum_{km\in L} B_{km,f} + \sum_{mn\in L} B_{mn,f}\right)\frac{V^{\mathrm{re}}_{m,f,t}}{2} = I^{\mathrm{Dim}}_{m,f,t} + I^{\mathrm{EVim}}_{m,f,t} \quad \forall m \in N, f \in F, t \in T \quad (3)$$

$$P^{D}_{n,f,t} = V^{\mathrm{re}}_{n,f,t} I^{\mathrm{Dre}}_{n,f,t} + V^{\mathrm{im}}_{n,f,t} I^{\mathrm{Dim}}_{n,f,t} \quad \forall n \in N, f \in F, t \in T \quad (4)$$

$$Q^{D}_{n,f,t} = -V^{\mathrm{re}}_{n,f,t} I^{\mathrm{Dim}}_{n,f,t} + V^{\mathrm{im}}_{n,f,t} I^{\mathrm{Dre}}_{n,f,t}, \forall n \in N, f \in F, t \in T \quad (5)$$

$$V^{\mathrm{re}}_{m,f,t} - V^{\mathrm{re}}_{n,f,t} = \sum_{h\in F}\left(R_{mn,f,h} I^{\mathrm{re}}_{mn,h,t} - X_{mn,f,h} I^{\mathrm{im}}_{mn,h,t}\right) \quad \forall mn \in L, f \in F, t \in T \quad (6)$$

$$V^{\mathrm{im}}_{m,f,t} - V^{\mathrm{im}}_{n,f,t} = \sum_{h\in F}\left(X_{mn,f,h} I^{\mathrm{re}}_{mn,h,t} + R_{mn,f,h} I^{\mathrm{im}}_{mn,h,t}\right) \quad \forall mn \in L, f \in F, t \in T \quad (7)$$

$$0 \le P^{G}_{n,t} \le \overline{P}^{G}_{n} \quad \forall n \in N, t \in T \quad (8)$$

$$\underline{Q}^{G}_{n} \le Q^{G}_{n,t} \le \overline{Q}^{G}_{n} \quad \forall n \in N, t \in T \quad (9)$$

$$\left|Q^{G}_{n,t}\right| \le P^{G}_{n,t} \tan(\arccos(pf_n)) \quad \forall n \in N, t \in T \quad (10)$$

$$\frac{P^{G}_{n,t}}{3} = V^{\mathrm{re}}_{n,f,t} I^{\mathrm{Gre}}_{n,f,t} + V^{\mathrm{im}}_{n,f,t} I^{\mathrm{Gim}}_{n,f,t} \quad \forall n \in N, f \in F, t \in T \quad (11)$$

$$\frac{Q^{G}_{n,t}}{3} = -V^{\mathrm{re}}_{n,f,t} I^{\mathrm{Gim}}_{n,f,t} + V^{\mathrm{im}}_{n,f,t} I^{\mathrm{Gre}}_{n,f,t}, \forall n \in N, f \in F, t \in T \quad (12)$$

$$\underline{V}^{2} \le {V^{\mathrm{re}}_{n,f,t}}^{2} + {V^{\mathrm{im}}_{n,f,t}}^{2} \le \overline{V}^{2} \quad \forall n \in N, f \in F, t \in T \quad (13)$$

$$0 \le {I^{\mathrm{re}}_{mn,f,t}}^{2} + {I^{\mathrm{im}}_{mn,f,t}}^{2} \le \bar{I}_{mn}{}^{2} \ \forall mn \in L, f \in F, t \in T \quad (14)$$

$$E^{\mathrm{EV}}_{n} = \sum_{t\in T} \Delta_t P^{\mathrm{EV}}_{n,t} \quad \forall n \in N \quad (15)$$

$$\overline{E}^{\mathrm{EV}}_{n} = E^{\mathrm{EV}}_{n} + E^{\mathrm{SoC}}_{n} + E^{SH}_{n} \quad \forall n \in N \quad (16)$$

$$P^{\mathrm{EV}}_{n,t} = \overline{P}^{\mathrm{EV}}_{n} y_{n,t} \quad \forall n \in N, t \in T \quad (17)$$

$$\frac{P^{\mathrm{EV}}_{n,t}}{3} = V^{\mathrm{re}}_{n,f,t} I^{\mathrm{EVre}}_{n,f,t} + V^{\mathrm{im}}_{n,f,t} I^{\mathrm{EVim}}_{n,f,t}, \forall n \in N, f \in F, t \in T \quad (18)$$

$$0 = -V^{\mathrm{re}}_{n,f,t} I^{\mathrm{EVim}}_{n,f,t} + V^{\mathrm{im}}_{n,f,t} I^{\mathrm{EVre}}_{n,f,t}, \forall n \in N, f \in F, t \in T \quad (19)$$

$$y_{n,t} = 0 \quad \forall n \in N, t \in T : t^{\mathrm{arr}}_{n} < t \vee t > t^{\mathrm{dep}}_{n} \quad (20)$$

$$y_{n,t} \in \{0, 1\} \quad \forall n \in N, t \in T. \quad (21)$$

The objective of the EVCC problem is to minimize the cost of the energy provided by the substation and the DGs, as shown in the first two terms of (1). The third term considered in the objective function represents the EVs energy curtailment if the EVs cannot be charged completely, while the fourth term is added to encourage the charging of priority EVs during the initial hours of the time period. The parameter ρ_t in the fourth term of the objective function is defined as $2\hat{}[6+24H(t-18)-t]$, in which $H(t)$ is the Heaviside step function. This parameter is a decreasing function of the time period that encourages the charging of a priority EV (EV with $\kappa_n = 1$) as soon as possible. The state of the EV charging at bus n in time interval t is determined by the binary decision variable $y_{n,t}$. If $y_{n,t}$ is 1, then the EV is charging in that time period, and if $y_{n,t}$ is zero, then the EV is not charging.

Constraints (2) and (3) represent the balance of the real and imaginary parts of the circuit currents, respectively. The currents demanded by the loads are determined by (4) and (5). Constraints (6) and (7) represent the application of Kirchoff's voltage law (KVL) for each independent loop in the EDS (formed by each circuit). So, (2) and (3) ensure compliance with Kirchoff's current law, while (6) and (7) ensure KVL compliance. The operation limits of the DGs are represented by (8)–(10), while (11) and (12) correspond to the definition of the active and reactive power of the DGs.

Constraints (13) and (14) represent the limits of the voltage magnitude and the current capacity of each circuit, respectively. The energy charged in the EV is represented by (15), while (16) establishes the energy balance between the EVs energy capacity, the energy charged, the initial energy state, and the energy curtailment. The power demanded by the EV depends on the charging state, associated with the binary variable $y_{n,t}$, as shown in (17). The active and reactive powers demanded by the EVs are defined by (18) and (19). Equation (20) allows the EV to be charged only during the time interval between arrival and departure defined by parameters t^{arr}_{n} and t^{dep}_{n}. Finally, the binary nature of the EVs charging state variables is represented by (21).

Note that (2)–(14) represent the steady-state operation of an unbalanced EDS considering the presence of DGs and it can be used to formulate mathematical models for other EDS optimization problems.

IV. Linearization of the MINLP Model for the EVCC Problem

Note that the active and reactive powers related to the loads in (4) and (5), the DGs in (11) and (12), and the EVs in (18) and (19), as well as the limits for voltage magnitude in (13) and current magnitude in (14), are nonlinear expressions. In this section, these equations will be linearized, in order to obtain a MILP for the EVCC problem.

A. Linearization of the Load Currents

The load currents must satisfy (4) and (5). Another way to write the relationship between power, voltage and current for the loads is shown in (22) and (23), in which g and h are nonlinear functions of the real and imaginary parts of the voltage.

$$I^{\mathrm{Dre}}_{n,f,t} = g\left(P^{D}_{n,f,t}, Q^{D}_{n,f,t}, V^{\mathrm{re}}_{n,f,t}, V^{\mathrm{im}}_{n,f,t}\right) = \frac{P^{D}_{n,f,t} V^{\mathrm{re}}_{n,f,t} + Q^{D}_{n,f,t} V^{\mathrm{im}}_{n,f,t}}{{V^{\mathrm{re}}_{n,f,t}}^{2} + {V^{\mathrm{im}}_{n,f,t}}^{2}}, \forall n \in N, f \in F, t \in T \quad (22)$$

$$I^{\mathrm{Dim}}_{n,f,t} = h\left(P^{D}_{n,f,t}, Q^{D}_{n,f,t}, V^{\mathrm{re}}_{n,f,t}, V^{\mathrm{im}}_{n,f,t}\right) = \frac{P^{D}_{n,f,t} V^{\mathrm{im}}_{n,f,t} - Q^{D}_{n,f,t} V^{\mathrm{re}}_{n,f,t}}{{V^{\mathrm{re}}_{n,f,t}}^{2} + {V^{\mathrm{im}}_{n,f,t}}^{2}}, \forall n \in N, f \in F, t \in T. \quad (23)$$

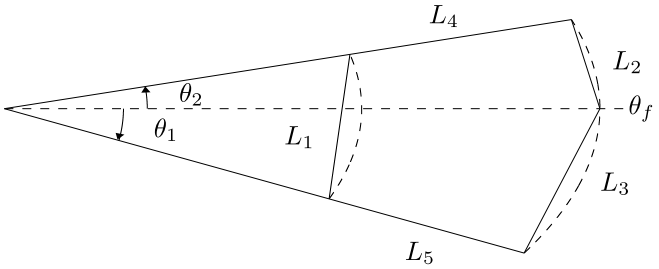

Fig. 1. Constraints for voltage limits (phase A).

As the voltage magnitude in an EDS has a relatively small and limited range of variation, (22) and (23) can be linearized around an estimated operation point ($V^{\text{re}*}_{n,f,t}$, $V^{\text{im}*}_{n,f,t}$), as shown in (24) and (25).

$$I^{\text{Dre}}_{n,f,t} = g^* + \frac{\partial g}{\partial V^{\text{re}}}\bigg|^* \left(V^{\text{re}}_{n,f,t} - V^{\text{re}*}_{n,f,t}\right) + \frac{\partial g}{\partial V^{\text{im}}}\bigg|^* \left(V^{\text{im}}_{n,f,t} - V^{\text{im}*}_{n,f,t}\right) \quad \forall n \in N, f \in F, t \in T \tag{24}$$

$$I^{\text{Dim}}_{n,f,t} = h^* + \frac{\partial h}{\partial V^{\text{re}}}\bigg|^* \left(V^{\text{re}}_{n,f,t} - V^{\text{re}*}_{n,f,t}\right) + \frac{\partial h}{\partial V^{\text{im}}}\bigg|^* \left(V^{\text{im}}_{n,f,t} - V^{\text{im}*}_{n,f,t}\right) \quad \forall n \in N, f \in F, t \in T. \tag{25}$$

So, linear equations (24) and (25) can be used to approximate the nonlinear expressions defined by (4) and (5). The error of the linear approximation is determined by the quality of the estimated operation point, which can be obtained using historical data, the knowledge of the EDS operator, or the previous state of the EDS.

B. Linearization of the Active and Reactive Powers of DGs and EVs

The active and reactive powers of the DGs represented by (11) and (12) and the active and reactive powers of the EVs modeled by (18) and (19) are approximated using an estimated operation point ($V^{\text{re}*}_{n,f,t}$, $V^{\text{im}*}_{n,f,t}$) as shown in (26)–(29).

$$\frac{P^G_{n,t}}{3} = V^{\text{re}*}_{n,f,t} I^{\text{Gre}}_{n,f,t} + V^{\text{im}*}_{n,f,t} I^{\text{Gim}}_{n,f,t} \quad \forall n \in N, f \in F, t \in T \tag{26}$$

$$\frac{Q^G_{n,t}}{3} = -V^{\text{re}*}_{n,f,t} I^{\text{Gim}}_{n,f,t} + V^{\text{im}*}_{n,f,t} I^{\text{Gre}}_{n,f,t}, \forall n \in N, f \in F, t \in T \tag{27}$$

$$\frac{P^{\text{EV}}_{n,t}}{3} = V^{\text{re}*}_{n,f,t} I^{\text{EVre}}_{n,f,t} + V^{\text{im}*}_{n,f,t} I^{\text{EVim}}_{n,f,t}, \forall n \in N, f \in F, t \in T \tag{28}$$

$$0 = -V^{\text{re}*}_{n,f,t} I^{\text{EVim}}_{n,f,t} + V^{\text{im}*}_{n,f,t} I^{\text{EVre}}_{n,f,t}, \forall n \in N, f \in F, t \in T. \tag{29}$$

C. Linearization of the Voltage Limits

Due to the fact that the phase angle variation around the reference voltage for each phase in the EDS is small, the voltage limits for phase A, defined by (13), can be represented using linear constraints (30)–(34), according to Fig. 1. Constraints (30)–(34) are related with lines L_1–L_5, respectively, and limit the voltage magnitudes between $[\underline{V}, \overline{V}]$ and the phase angles between $[\theta_f - \theta_1, \theta_f + \theta_2]$. The vector of reference phase angles θ is $[0°, +120°, -120°]$ for phases A, B, and C; θ_1 and θ_2 are the maximum negative and the maximum positive deviation of the phase angle around the reference for each phase. The voltage limits for phases B and C are linearized by using similar constraints.

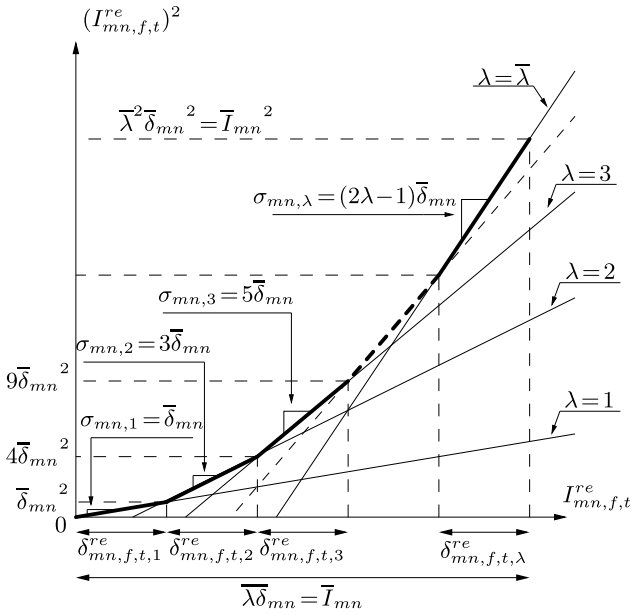

Fig. 2. Modeling the piecewise linear $(I^{\text{re}}_{mn,f,t})^2$ function.

$$V^{\text{im}}_{n,f,t} \le \frac{\sin(\theta_f+\theta_2)-\sin(\theta_f-\theta_1)}{\cos(\theta_f+\theta_2)-\cos(\theta_f-\theta_1)}\left[V^{\text{re}}_{n,f,t} - \underline{V}\cos(\theta_f+\theta_2)\right] + \underline{V}\sin(\theta_f+\theta_2) \quad \forall n \in N, f = A, t \in T \tag{30}$$

$$V^{\text{im}}_{n,f,t} \le \frac{\sin(\theta_f+\theta_2)-\sin\theta_f}{\cos(\theta_f+\theta_2)-\cos\theta_f}\left[V^{\text{re}}_{n,f,t} - \overline{V}\cos\theta_f\right] + \overline{V}\sin\theta_f \quad \forall n \in N, f = A, t \in T \tag{31}$$

$$V^{\text{im}}_{n,f,t} \ge \frac{\sin(\theta_f-\theta_1)-\sin\theta_f}{\cos(\theta_f-\theta_1)-\cos\theta_f}\left[V^{\text{re}}_{n,f,t} - \overline{V}\cos\theta_f\right] + \overline{V}\sin\theta_f \quad \forall n \in N, f = A, t \in T \tag{32}$$

$$V^{\text{im}}_{n,f,t} \le V^{\text{re}}_{n,f,t}\tan(\theta_f+\theta_2) \quad \forall n \in N, f = A, t \in T \tag{33}$$

$$V^{\text{im}}_{n,f,t} \ge V^{\text{re}}_{n,f,t}\tan(\theta_f-\theta_1) \quad \forall n \in N, f = A, t \in T. \tag{34}$$

D. Linearization of the Current Limit Constraint

The current limit constraint, represented by (14), is linearized using (35)–(42), as is shown in [23] (see Fig. 2). In (35), the terms $\sum_{\lambda=1}^{\overline{\lambda}} \sigma_{mn,\lambda}\delta^{\text{re}}_{mn,f,t,\lambda}$ and $\sum_{\lambda=1}^{\overline{\lambda}} \sigma_{mn,\lambda}\delta^{\text{im}}_{mn,f,t,\lambda}$ are the linear approximations of $(I^{\text{re}}_{mn,f,t})^2$ and $(I^{\text{im}}_{mn,f,t})^2$, respectively, where $\sigma_{mn,\lambda}$ and $\overline{\delta}_{mn}$ are constant parameters, as defined by (43) and (44).

$$I^{\text{sqr}}_{mn,f,t} = \sum_{\lambda=1}^{\overline{\lambda}} \sigma_{mn,\lambda}\delta^{\text{re}}_{mn,f,t,\lambda} + \sum_{\lambda=1}^{\overline{\lambda}} \sigma_{mn,\lambda}\delta^{\text{im}}_{mn,f,t,\lambda} \quad \forall mn \in L, f \in F, t \in T \tag{35}$$

$$I^{\text{re}}_{mn,f,t} = I^{\text{re}+}_{mn,f,t} - I^{\text{re}-}_{mn,f,t} \quad \forall mn \in L, f \in F, t \in T \tag{36}$$

$$I^{\text{im}}_{mn,f,t} = I^{\text{im}+}_{mn,f,t} - I^{\text{im}-}_{mn,f,t} \quad \forall mn \in L, f \in F, t \in T \tag{37}$$

$$I^{\text{re}+}_{mn,f,t} + I^{\text{re}-}_{mn,f,t} = \sum_{\lambda=1}^{\overline{\lambda}} \delta^{\text{re}}_{mn,f,t,\lambda}, \quad \forall mn \in L, f \in F, t \in T \tag{38}$$

$$I^{\text{im}+}_{mn,f,t} + I^{\text{im}-}_{mn,f,t} = \sum_{\lambda=1}^{\overline{\lambda}} \delta^{\text{im}}_{mn,f,t,\lambda}, \quad \forall mn \in L, f \in F, t \in T \tag{39}$$

$$0 \le \delta^{\text{re}}_{mn,f,t,\lambda} \le \overline{\delta}_{mn}, \forall mn \in L, f \in F, t \in T, \lambda = 1 \ldots \overline{\lambda} \quad (40)$$

$$0 \le \delta^{\text{im}}_{mn,f,t,\lambda} \le \overline{\delta}_{mn}, \forall mn \in L, f \in F, t \in T, \lambda = 1 \ldots \overline{\lambda} \quad (41)$$

$$I^{\text{re}+}_{mn,f,t}, I^{\text{re}-}_{mn,f,t}, I^{\text{im}+}_{mn,f,t}, I^{\text{im}-}_{mn,f,t} \ge 0 \quad \forall mn \in L, f \in F, t \in T \quad (42)$$

$$\sigma_{mn,\lambda} = (2\lambda - 1)\overline{\delta}_{mn} \quad \forall mn \in L, \lambda = 1 \ldots \overline{\lambda} \quad (43)$$

$$\overline{\delta}_{mn} = \frac{\overline{I}_{mn}}{\overline{\lambda}} \quad \forall mn \in L. \quad (44)$$

V. Mixed-Integer LP Model for the EVCC Problem

The EVCC problem is modeled as a MILP problem as follows:

$$\min \quad (1)$$

subject to: (2)–(3), (6)–(10), (15)–(17), (21), and (24)–(44)

$$0 \le I^{\text{sqr}}_{mn,f,t} \le \overline{I}^2_{mn} \quad \forall mn \in L, f \in F, t \in T. \quad (45)$$

The proposed MILP model is more robust than a MINLP model, and the application of classical optimization techniques can guarantee to find the optimal solution to the problem.

The quality of the linear approximations can be adjusted by using a suitable estimated operation point and by increasing the number $\overline{\lambda}$ of discretization blocks used in the square current linearization. The estimated operation point used in the linearized equations was obtained by solving a linear relaxation of the MILP model in which the binary nature of the decision variables was temporarily disregarded. The solution of that relaxed model (a linear programming problem) defined the estimated operation point.

VI. Tests and Results

The proposed model was tested in a 394-nodes distribution system with 34 nodes at a medium voltage level (13.8 kV) and 360 nodes at a low voltage level (220 V). The distribution system at the medium voltage level was based on the data in [22]. The maximum and minimum voltage magnitude limits were 1.00 and 0.90 p.u., respectively. The voltage magnitude at the substation was fixed at 1p.u. The energy capacity of the EV batteries was 50 kWh with a maximum power of 10 kW (these values were based on information provided in [24]). It must be clarified that the parameter $\overline{E}_n$, which represents the energy capacity of the EV at node n, is the energy that can actually be stored in the battery, rather than its nominal capacity.

The parameter $\overline{\lambda}$ was set at 10, while $\overline{I}_{mn}$ was 200 A for all feeders. The time period considered went from 18:00 to 08:00 h, and the time intervals had a duration of 1 h. The parameters θ_1 and θ_2 were 3° and 1°, while β was 10 U.S.$/kWh. The hourly energy cost and load variation percentage is shown in Table I.

The distribution system considered a three-phase model with secondary networks connected through medium voltage level nodes, as shown in Fig. 3. The topology of the secondary networks is represented in Fig. 4. The medium voltage node where the transformer for each secondary network was connected, is represented as "xx" in Fig. 4. The test system had 18 secondary networks connected at nodes 4, 9, 11, 13, 14, 17, 18, 20, 22, 24–26, and 28–33. The total conventional demand of the system is 597.5, 630.8, and 566.8 kVA, connected in phases A, B, and C, respectively. So, phases A, B, and C are charged with 33.3%, 35.1%, and 31.6% of the total demand, respectively.

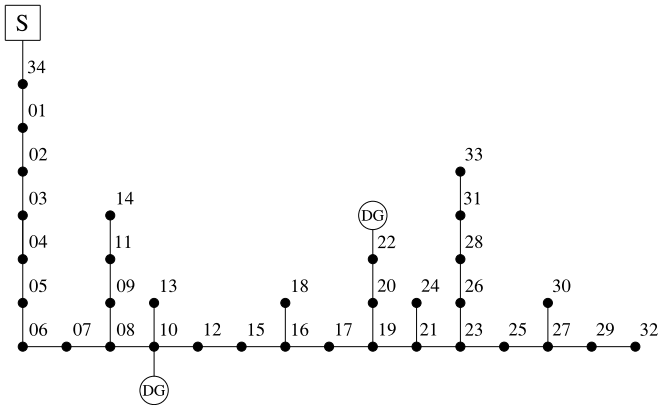

Fig. 3. Topology of the medium voltage level network.

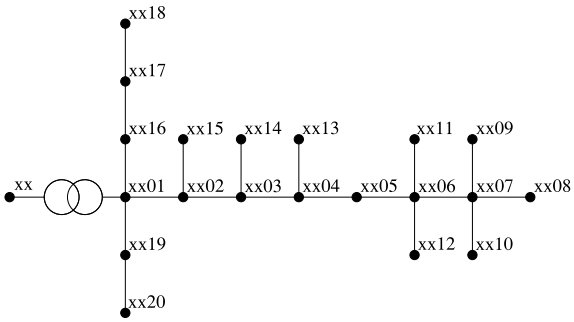

Fig. 4. Topology of the secondary networks.

The model was implemented in A Mathematical Programming Language [25] and solved with CPLEX [26] using a computer with an Intel i7 4770 processor. The time limit for the solution process was 600 s.

A. Tests Considering Balance in the Connection of the EVs to the EDS

Tests were carried out considering two EV penetration percentages in the system, named as EV15% and EV40%. In the case of EV15%, there were EVs at nodes xx2, xx15, and **xx17**, while in the case of EV40%, there were EVs at the secondary network nodes xx2, xx6, xx8, **xx10**, xx15, **xx17**, xx18, and xx20 (nodes in bold indicate priority EVs). The EV penetration percentage corresponded to the ratio of low voltage nodes with the presence of EVs, considering one vehicle per bus. Additional tests were performed considering the presence of +DG, without the priority option (+w/oP) and without the voltage limit constraint (+w/oVL). For these cases, it is assumed that the EVs are connected uniformly in the phases of the EDS.

In the cases marked with +DG, the EDS had two DGs connected at nodes 10 and 22, with energy costs $\alpha^G_{n,t}$ equal to 0.04 U.S.$/kWh, maximum active power of 500 kW, and minimum and maximum reactive power equal to −200 and 200 kVAr. The minimum power factor for the operation of the DGs was 0.90.

TABLE I
ENERGY COST AND LOAD VARIATION FOR THE TEST SYSTEM

Hour	$\alpha^S_{n,t}$ ($/kWh)	% of peak load	Hour	$\alpha^S_{n,t}$ ($/kWh)	% of peak load
18:00	0.066	99	01:00	0.036	40
19:00	0.070	93	02:00	0.034	37
20:00	0.075	91	03:00	0.030	35
21:00	0.077	87	04:00	0.028	33
22:00	0.070	75	05:00	0.027	33
23:00	0.060	65	06:00	0.027	41
24:00	0.048	55	07:00	0.029	44

TABLE II
SUMMARY OF THE TEST CASES

Case	Objective Function	Energy Cost	Total E^{SH}_n	Priority Benefit	Time (s)
EV15%	-813121.81	958.19 (-0.003%)	0	814080	137
EV15%+DG	-1427740.48	739.52 (-0.020%)	0	1428480	49
EV15%+w/oVL	-1427520.13	959.87 (-0.002%)	0	1428480	35
EV15%+w/oP	915.06	915.06 (-0.003%)	0	0	61
EV40%	-1123190.53	1129.47 (-0.036%)	0	1124320	600
EV40%+DG	-2856039.86	920.14 (-0.020%)	0	2856960	51
EV40%+w/oVL	-2855814.27	1145.73 (-0.044%)	0	2856960	36
EV40%+w/oP	1059.81	1059.81 (-0.023%)	0	0	600

Table II shows a summary of the results from the test cases. For all of the tests, the resultant EV charging schedule had no energy curtailment, which means that all of the EVs were completely charged by the end of the time period. Most of the cases were solved within the time limit, except the cases EV40% and EV40%+w/oP, in which the solution process finished with gap values of 0.01% and 0.16%, respectively (a low gap value guarantees that the solution is very close to the optimal solution). When those cases were solved without a time limit, it was verified that the solution found was actually the optimal solution for each case, which shows the efficiency of the proposed method.

In order to evaluate the precision of the proposed MILP model, the objective function of the optimal charging schedule for each case was calculated using a conventional ac load flow. The percentage error of the energy cost calculated by the MILP model is shown in parentheses in Table II. The low percentage of errors indicates that the linearizations carried out to obtain the MILP model are suitable.

The generated power of the substation and the DGs for each test case are shown in Figs. 5–12. The power related to the charging of priority EVs is shown in red, while the power related to the other EVs is shown in blue.

The best objective functions were obtained in the cases +DG and +w/oVL because the optimization model had the flexibility to operate using the power of the DGs or to permit voltages below the minimum limits. In those cases, the priority benefit may be higher due to the fast charging of the priority EVs. Additionally, the best charging schedule was obtained in the cases +DG because the DGs made it possible to operate with low energy costs and energy losses

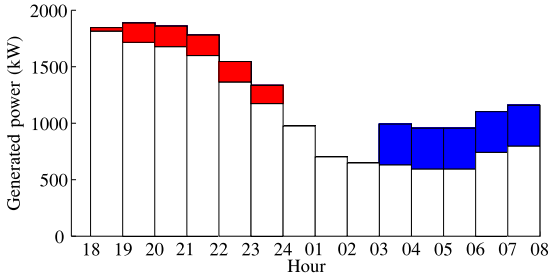

Fig. 5. Generated power for the case EV15%.

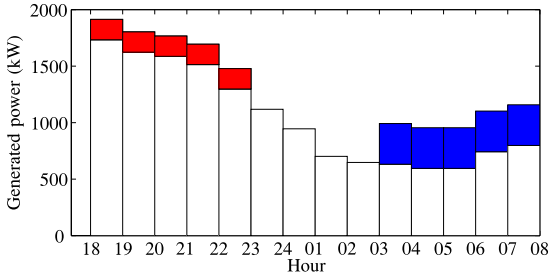

Fig. 6. Generated power for the case EV15%+DG.

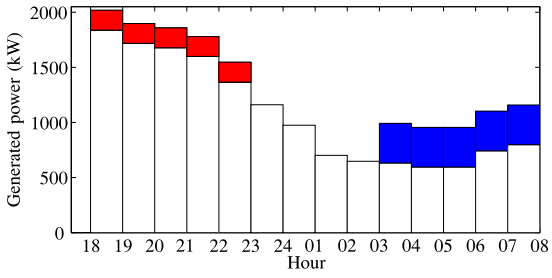

Fig. 7. Generated power for the case EV15%+w/oVL.

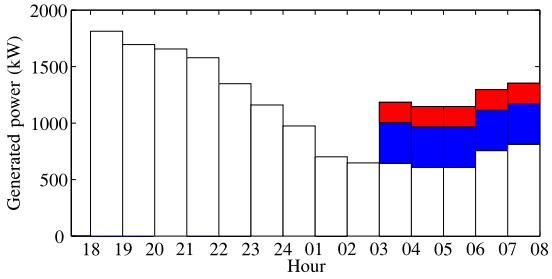

Fig. 8. Generated power for the case EV15%+w/oP.

were reduced. By contrast, the cases in which the priority option was not considered (+w/oP) had worse objective functions because there was no priority benefit to encourage quick charging of the priority EVs. However, the cases +w/oP had lower energy costs, as the optimization model could schedule the charging process in the time intervals with lower energy costs.

The minimum voltage is shown in Figs. 13 and 14 for the test cases with EV penetration percentages of 15% and 40%, respectively. The operation of the system without EVs was labeled as "EDS w/o EV." For all cases, the minimum voltage was at phase B. For all cases considering the voltage constraints, the voltage was above its minimum limit,

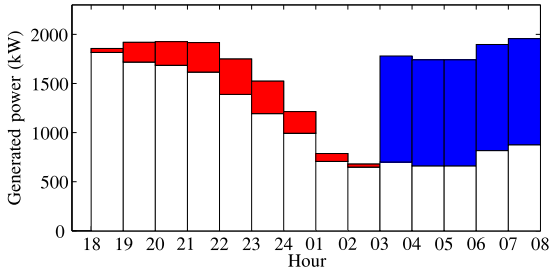

Fig. 9. Generated power for the case EV40%.

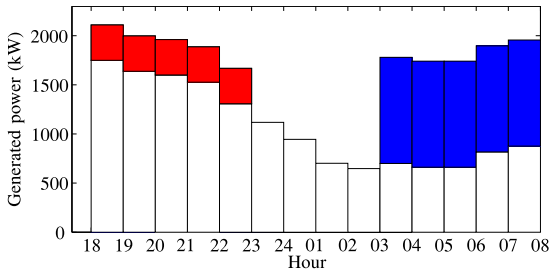

Fig. 10. Generated power for the case EV40%+DG.

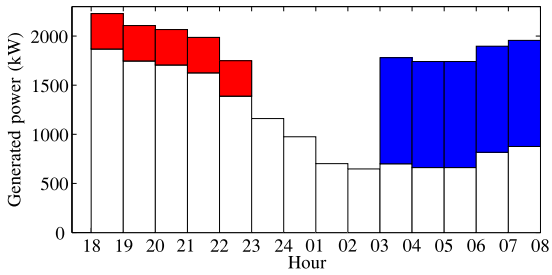

Fig. 11. Generated power for the case EV40%+w/oVL.

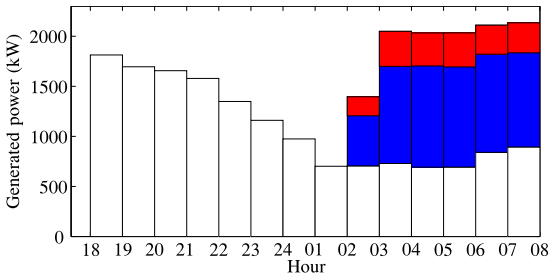

Fig. 12. Generated power for the case EV40%+w/oP.

except between the hours 18:00 and 19:00, in which the voltage was slightly below the minimum limit. But, since the voltage was very close to the minimum limit, those values could be accepted; the exceptions were solutions of the MILP model due to the linear approximations made in the voltage constraints, as shown in Fig. 1; as the phase angle variation was low, that linear approximation had a low level of error.

For cases without the voltage limit, the minimum voltage was below its limit, making it possible to obtain a better value for the objective function.

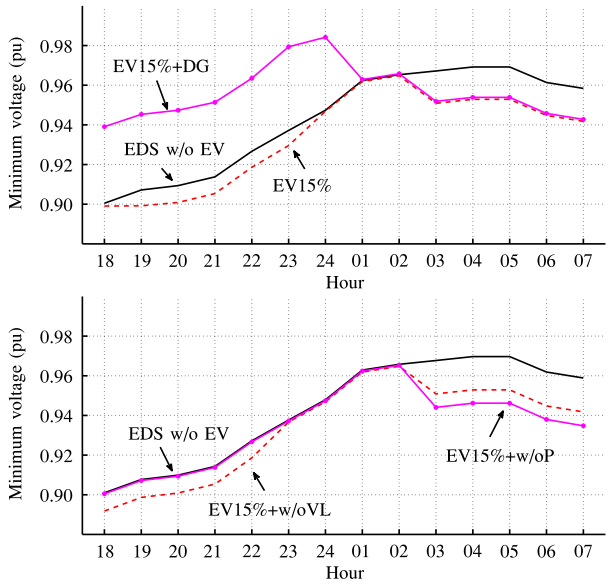

Fig. 13. Voltage profile for the cases with 15% EV penetration.

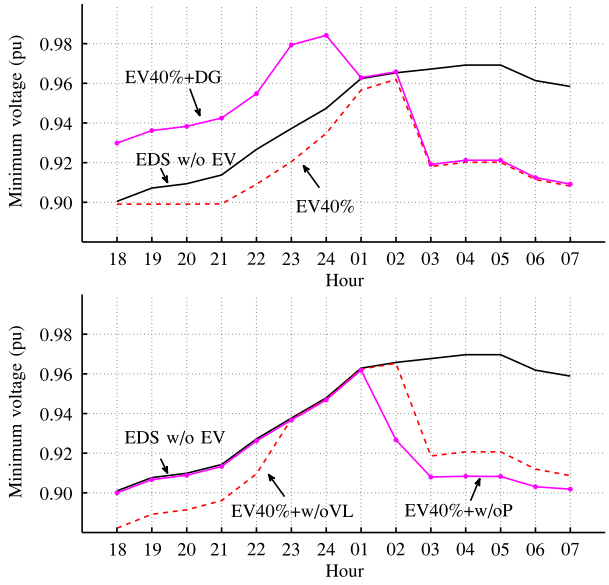

Fig. 14. Voltage profile for the cases with 40% EV penetration.

B. Tests Considering Imbalance in the Connection of the EVs to the EDS

The previous tests considered an ideal case in which the EVs were connected uniformly to the EDS. In this subsection, additional tests considering an imbalance in the connection of the EVs to the system (+imb) are presented. These tests were carried out for the case EV40% in order to illustrate the effects of the unbalanced connection of the EVs. In these tests, 34.7% of the EVs were connected to phase A, 38.9% were connected to phase B, and 26.4% were connected to phase C. A special test named +DG* was carried out considering the DG energy cost $\alpha^G_{n,t}$ as equal to 0.025 U.S.$/kWh in order to study the effect of the DG energy cost variation on the charging of EVs.

Table III shows a summary of the results from the test cases. For all of the tests, the resultant EV charging schedule had no

TABLE III
SUMMARY OF THE TEST CASES CONSIDERING IMBALANCE ON THE EVS

Case	Objective Function	Energy Cost	Total E_n^{SH}	Priority Benefit	Time (s)
EV40%+imb	-2094523.53	1156.47 (-0.065%)	0	2095680	600
EV40%+imb+DG	-2856023.02	936.98 (0.106%)	0	2856960	444
EV40%+imb+DG*	-2856188.24	771.76 (-0.539%)	0	2856960	317
EV40%+imb+w/oVL	-2855811.65	1148.35 (-0.100%)	0	2856960	221
EV40%+imb+w/oP	1073.81	1073.81 (-0.028%)	0	0	600

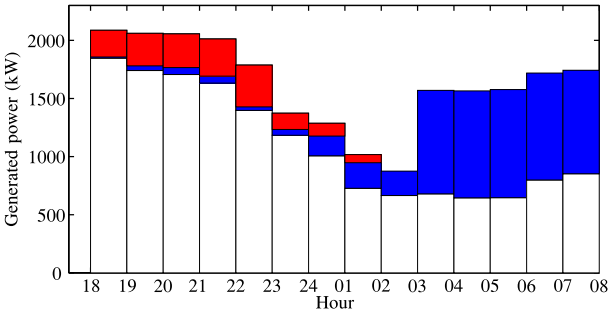

Fig. 15. Generated power for the case EV40%+imb.

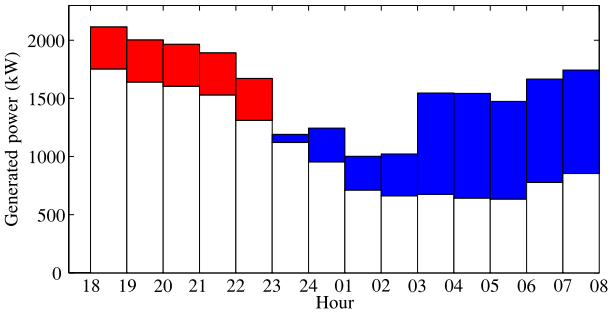

Fig. 16. Generated power for the case EV40%+imb+DG.

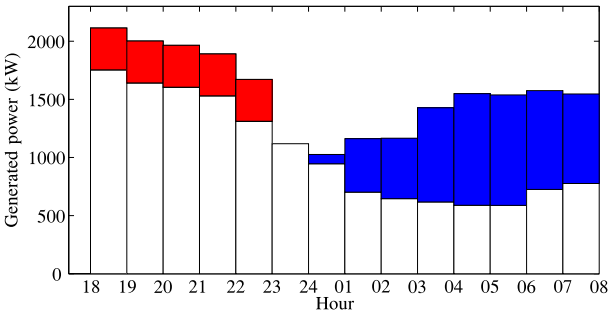

Fig. 17. Generated power for the case EV40%+imb+DG*.

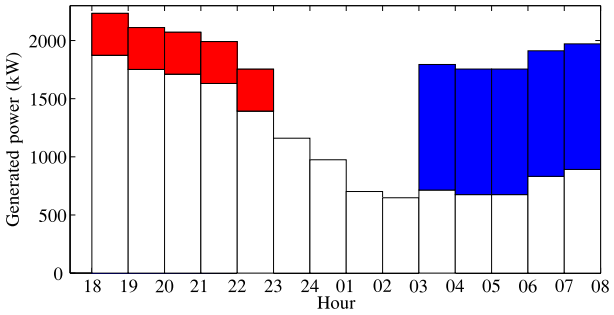

Fig. 18. Generated power for the case EV40%+imb+w/oVL.

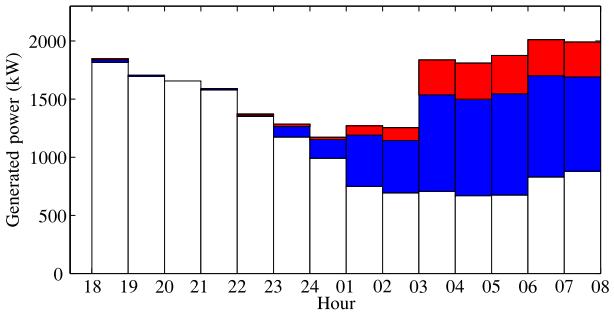

Fig. 19. Generated power for the case EV40%+imb+w/oP.

TABLE IV
MINIMUM VOLTAGE FOR THE UNBALANCED EV40% CASES (P.U.)

Hour	EDS w/o EV	EV40%+imb	EV40%+imb +DG
18:00	0.9005 (B)	0.9001 (C)	0.9179 (A)
19:00	0.9072 (B)	0.8998 (B)	0.9236 (A)
20:00	0.9094 (B)	0.8996 (B)	0.9255 (A)
21:00	0.9138 (B)	0.8998 (B)	0.9293 (A)
22:00	0.9267 (B)	0.9009 (A)	0.9404 (A)
23:00	0.9372 (B)	0.9185 (B)	0.9661 (B)
24:00	0.9474 (B)	0.9076 (B)	0.9520 (B)
01:00	0.9624 (B)	0.9198 (B)	0.9316 (B)
02:00	0.9653 (B)	0.9318 (B)	0.9289 (B)
03:00	0.9672 (B)	0.9107 (B)	0.9086 (B)
04:00	0.9692 (B)	0.9103 (B)	0.9105 (B)
05:00	0.9692 (B)	0.9116 (B)	0.9181 (B)
06:00	0.9614 (B)	0.9045 (B)	0.9126 (B)
07:00	0.9584 (B)	0.9044 (B)	0.9042 (B)
Hour	EV40%+imb +w/oVL	EV40%+imb +w/oP	EV40%+imb +DG*
18:00	0.8741 (A)	0.8999 (B)	0.9179 (A)
19:00	0.8804 (A)	0.9056 (B)	0.9236 (A)
20:00	0.8824 (A)	0.9094 (B)	0.9255 (A)
21:00	0.8865 (A)	0.9093 (B)	0.9293 (A)
22:00	0.8986 (A)	0.9176 (B)	0.9404 (A)
23:00	0.9372 (B)	0.9160 (B)	0.9791 (B)
24:00	0.9474 (B)	0.9228 (B)	0.9827 (B)
01:00	0.9624 (B)	0.9060 (B)	0.9517 (B)
02:00	0.9653 (B)	0.9145 (B)	0.9590 (B)
03:00	0.8813 (B)	0.9080 (B)	0.9422 (B)
04:00	0.8837 (B)	0.9119 (B)	0.9382 (B)
05:00	0.8837 (B)	0.9123 (B)	0.9374 (B)
06:00	0.8739 (B)	0.9029 (B)	0.9359 (B)
07:00	0.8702 (B)	0.9007 (B)	0.9384 (B)

energy curtailment. It can be noted that due to the imbalance of the EVs on the system The generated power of the substation and the DGs for these unbalanced cases are shown in Figs. 15–19. The priority benefit for the case EV40%+imb was larger than the one for the case EV40%, which means that some priority vehicles were charged more quickly (those in phases different from the more loaded phase B). However, the energy cost was increased because nonpriority vehicles were charged before 3:00 h at a higher energy cost.

The minimum voltage is shown in Table IV and Fig. 20. In Table IV, the phase with the minimum voltage is shown between parentheses; for these cases, the minimum voltage did not always occur at phase B. As shown in Tables III and IV, the solution for the unbalanced cases presented greater energy

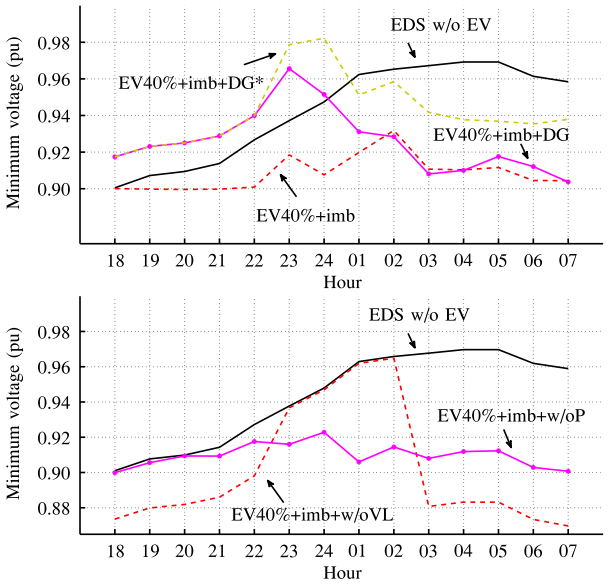

Fig. 20. Voltage profile for the cases with 40% unbalanced EV penetration.

costs and lower minimum voltages than for the ideal balanced cases.

In the case EV40%+imb+DG*, the DGs generated power at full capacity for almost the entire time period because their energy cost was lower than that of the substation. Moreover, analyzing Figs. 16 and 17 for the cases EV40%+imb+DG and EV40%+imb+DG*, it can be concluded that if the energy cost of the DGs is lower than that of the substation, then the charging of the EVs can be changed to take advantage of that lower cost, leading to a cheaper EV charging cost.

The case EV40%+imb+w/oVL can be considered as a "non-smart" charging schedule in terms of the EDS operation because the EVs were charged disregarding the voltage limits, which led to a violation of the operational constraints. Furthermore, if all EVs have priority, the charging will be carried out during the first hours of the time period, causing the worst operational conditions for the EDS. Therefore, a coordinated charging schedule for the EVs is necessary to guarantee the suitable operation of the EDS.

VII. Conclusion

A novel MILP model for the EVCC problem in EDS was presented. The proposed formulation can be used to obtain the optimal charging schedule for the charging of EV batteries, in order to achieve more economical operation of the EDS, while satisfying operational constraints. The employed three-phase representation of the EDS, based on current injections, makes it possible to adequately consider the imbalance of real distribution systems.

The MILP formulation was obtained after applying linearization techniques to a mixed integer nonlinear model. The low level of errors found in the test shows that the approximations are suitable and lead to a MILP model, which can be solved efficiently.

The application of a priority scheme allows users to choose between charging the batteries as quickly as possible or charging them with a minimum energy cost. The results show that the proposed method is efficient and can be used in the solution of the EVCC problem in EDSs.

Results showed that unbalanced EVs lead to a deterioration of the voltage profile and an increase in the energy cost. For this reason, the imbalance of the EVs in the EDS must be considered in the charging coordination problem.

The energy capacity used in the tests is greater than the average daily use of EVs and therefore the impact of EVs on the EDS may be overestimated. This value for the battery capacity of an EV was chosen in order to evaluate the worst case scenario and to demonstrate that the proposed method is able to find a feasible and optimal solution for this case.

Acknowledgment

The authors would like to thank FAPESP for fellowships and funding. They would also like to thank the IBM Academic Initiative for the CPLEX solver.

References

[1] T. Bevis, B. Hacker, C. S. Edrington, and S. Azongha, "A review of PHEV grid impacts," in *Proc. North Amer. Power Symp. (NAPS)*, Starkville, MS, USA, 2009, pp. 1–6.

[2] A. Y. Saber and G. K. Venayagamoorthy, "One million plug-in electric vehicles on the road by 2015," in *Proc. 12th Int. IEEE Conf. Intell. Transp. (ITSC)*, St. Louis, MO, USA, 2001, pp. 141–147.

[3] S. Lin, Z. He, T. Zang, and Q. Qian, "Impact of plug-in hybrid electric vehicles on distribution systems," in *Proc. Int. Conf. Power Syst. Technol. (POWERCON)*, Hangzhou, China, 2010, pp. 1–5.

[4] J. Schlee *et al.*, "The effects of plug-in electric vehicles on a small distribution grid," in *Proc. North Amer. Power Symp. (NAPS)*, Starkville, MS, USA, 2009, pp. 1–6.

[5] S. Sojoudi and S. H. Low, "Optimal charging of plug-in hybrid electric vehicles in smart grids," in *Proc. IEEE Power Energy Soc. (PES) Gen. Meeting*, Detroit, MI, USA, 2011, pp. 1–6.

[6] A. Trippe, T. Massier, and T. Hamacher, "Optimized charging of electric vehicles with regard to battery constraints—Case study: Singaporean car park," in *Proc. IEEE Energytech*, Cleveland, OH, USA, 2013, pp. 1–6.

[7] S. Deilami, A. S. Masoum, P. S. Moses, and M. A. S. Masoum, "Real-time coordination of plug-in electric vehicle charging in smart grids to minimize power losses and improve voltage profile," *IEEE Trans. Smart Grid*, vol. 2, no. 3, pp. 456–467, Sep. 2011.

[8] P. Richardson, D. Flynn, and A. Keane, "Optimal charging of electric vehicles in low-voltage distribution systems," *IEEE Trans. Power Syst.*, vol. 27, no. 1, pp. 268–279, Feb. 2012.

[9] M. D. Galus, R. A. Waraich, and G. Andersson, "Predictive, distributed, hierarchical charging control of PHEVs in the distribution system of a large urban area incorporating a multiagent transportation simulation," in *Proc. 17th Power Syst. Comput. Conf.*, Stockholm, Sweden, 2011, pp. 1–7.

[10] J. R. Pillai and B. Bak-Jensen, "Integration of vehicle-to-grid in the western Danish power system," *IEEE Trans. Sustain. Energy*, vol. 2, no. 1, pp. 12–19, Jan. 2011.

[11] E. Sortomme and M. A. El-Sharkawi, "Optimal charging strategies for unidirectional vehicle-to-grid," *IEEE Trans. Smart Grid*, vol. 2, no. 1, pp. 131–138, Mar. 2011.

[12] H. Sekyung, H. Soohee, and K. Sezaki, "Development of an optimal vehicle-to-grid aggregator for frequency regulation," *IEEE Trans. Smart Grid*, vol. 1, no. 1, pp. 65–72, Jun. 2010.

[13] R. M. Patil, J. C. Kelly, Z. Filipi, and H. K. Fathy, "A framework for the integrated optimization of charging and power management in plug-in hybrid electric vehicles," *IEEE Trans. Veh. Technol.*, vol. 62, no. 6, pp. 2402–2412, Jul. 2013.

[14] P. Sanchez-Martin, G. Sanchez, and G. Morales-Espana, "Direct load control decision model for aggregated EV charging points," *IEEE Trans. Power Syst.*, vol. 27, no. 3, pp. 1577–1584, Aug. 2012.

[15] D. Papadaskalopoulos, P. Mancarella, M. Aunedi, V. Stanojevic, and G. Strbac, "Decentralized participation of flexible demand in electricity markets—Part II: Application with electric vehicles and heat pump systems," *IEEE Trans. Power Syst.*, vol. 28, no. 4, pp. 3667–3774, Nov. 2013.

[16] R. Shankar and J. Marco, "Method for estimating the energy consumption of electric vehicles and plug-in hybrid electric vehicles under real-world driving conditions," *IET Intell. Transp. Syst.*, vol. 7, no. 1, pp. 138–150, Mar. 2013.

[17] A. Mohamed, V. Salehi, T. Ma, and O. Mohammed, "Real-time energy management algorithm for plug-in hybrid electric vehicle charging parks involving sustainable energy," *IEEE Trans. Sustain. Energy*, vol. 5, no. 2, pp. 577–586, Apr. 2014.

[18] P. Rezaei, J. Frolik, and P. D. H. Hines, "Packetized plug-in electric vehicle charge management," *IEEE Trans. Smart Grid*, vol. 5, no. 2, pp. 642–650, Mar. 2014.

[19] J. D. Melo, E. M. Carreño, and A. Padilha-Feltrin, "Spatial-temporal simulation to estimate the load demand of battery electric vehicles charging in small residential areas," *J. Control Autom. Elect. Syst.*, vol. 25, no. 4, pp. 470–480, 2014.

[20] K. Qian, C. Zhou, M. Alan, and Y. Yuan, "Modeling of load demand due to EV battery charging in distribution systems," *IEEE Trans. Power Syst.*, vol. 26, no. 2, pp. 802–810, May 2011.

[21] A. Lojowska, D. Kurowicka, G. Papaefthymiou, and L. van der Sluis, "Stochastic modeling of power demand due to EVs using copula," *IEEE Trans. Power Syst.*, vol. 27, no. 4, pp. 1960–1968, Nov. 2012.

[22] (Aug. 2011). *IEEE PES Distribution Test Feeders, 34-bus Feeder*. [Online]. Available: http://ewh.ieee.org/soc/pes/dsacom/testfeeders/index.html

[23] J. F. Franco, M. J. Rider, M. Lavorato, and R. Romero, "A mixed-integer LP model for the reconfiguration of radial electric distribution systems considering distributed generation," *Elect. Power Syst. Res.*, vol. 97, pp. 51–60, Apr. 2013.

[24] (May, 1, 2014). *Tesla Motors—Model Specifications*. [Online]. Available: http://www.teslamotors.com/models/specs

[25] R. Fourer, D. M. Gay, and B. W. Kernighan, *AMPL: A Modeling Language for Mathematical Programming*, 2nd Ed. Pacific Grove, CA, USA: Brooks/Cole-Thomson, 2003.

[26] *IBM ILOG CPLEX V12.1 User's Manual for CPLEX*, CPLEX Division, ILOG, Incline Village, NV, USA, 2009.

John F. Franco (S'11–M'13) received the B.Sc. and M.Sc. degrees in electrical engineering from the Universidad Tecnológica de Pereira, Pereira, Colombia, in 2004 and 2006, respectively, and the Ph.D. degree in electrical engineering from São Paulo State University (UNESP), Ilha Solteira, Brazil, in 2012.

His current research interests include the development of methodologies for the optimization, planning, and control of electrical power systems.

Marcos J. Rider (S'97–M'06) received the B.Sc. (Hons.) and P.E. degrees in electrical engineering from the National University of Engineering, Lima, Perú, in 1999 and 2000, respectively; the M.Sc. degree from the Federal University of Maranhão, Maranhão, Brazil, in 2002; and the Ph.D. degree from the University of Campinas, Campinas, Brazil, in 2006, all in electrical engineering.

He is currently a Professor with the Department of Electrical Engineering, São Paulo State University (FEIS-UNESP), Ilha Solteira, Brazil. His current research interests include the development of methodologies for the optimization, planning, and control of electrical power systems, and applications of artificial intelligence in power systems.

Ruben Romero (M'93–SM'08) received the B.Sc. and P.E. degrees in electrical engineering from the National University of Engineering, Lima, Perú, in 1978 and 1984, respectively, and the M.Sc. and Ph.D. degrees from the University of Campinas, Campinas, Brazil, in 1990 and 1993, respectively.

He is currently a Professor with the Department of Electrical Engineering, São Paulo State University (FEIS-UNESP), Ilha Solteira, Brazil. His current research interests include electrical power systems planning.